Optical, Magnetic and Structural Properties of the Spin-Crossover Complex [Fe(btr)$_2$(NCS)$_2$]·H$_2$O in the Light-Induced and Thermally Quenched Metastable States

Vincent Legrand,[a,b] Sébastien Pillet,[a] Chiara Carbonera,[c] Mohamed Souhassou,[a] Jean-François Létard,[c] Philippe Guionneau,[c] and Claude Lecomte*[a]

[Fe(btr)$_2$(NCS)$_2$]·H$_2$O [btr = 4,4′-bis(1,2,4-triazole)] is the archetype of highly cooperative and low-dimensional spin-crossover complexes, which exhibit low-spin (LS) to high-spin (HS) light-induced conversion at very low temperature. The structural reorganizations related to the light-induced and thermally induced LS–HS transitions were characterized by single-crystal X-ray diffraction below the relaxation temperature ($T = 15$ K $< T_{\text{LIESST}}$) and at 130 K within the thermal hysteresis loop. We show that the LIESST and thermal spin transitions lead to the same structural variations, namely an elongation of the Fe–N bonds by 0.18 Å (Fe–N$_{\text{NCS}}$) and 0.20 Å (Fe–N$_{\text{btr}}$), on going from LS to HS, together with a reorientation of the NCS group by nearly 13°. The atomic displacement amplitudes, derived from the crystal structures,

indicate lattice vibration modes of larger amplitudes and correlatively lower vibration frequencies in the HS state. The deformation of the crystal lattice as a function of temperature and laser excitation was quantitatively analyzed in terms of the HS and LS thermal-expansion (α_{HS} and α_{LS}) and spin-transition spontaneous-strain (ϵ) tensors. The eigendirections and eigenvalues of the α and ϵ tensors correlate well with the weak and strong interactions in the solid and are responsible for the high cooperativity and low-dimensional behaviour. Magnetic and spectroscopic measurements were performed in all the different spin states and related to the structural findings.

Keywords: Iron(II) / Photoswitching / Structural analysis / Photomagnetism / Spin crossover

Introduction

Spin crossover in iron(II) coordination complexes is a quite well-understood phenomenon, which has been thoroughly described and reviewed in the literature.[1] The spin conversion is related to the change in the electronic configuration of iron from $t_{2g}^4 e_g^2$ in the high-spin (HS) state to $t_{2g}^6 e_g^0$ in the low-spin (LS) state on decreasing temperature. This HS→LS electron redistribution in general parallels drastic structural modifications, namely a contraction of the Fe–ligand bonds by typically 0.2 Å as well as a decrease in the distortion of the Fe octahedral coordination polyhedron.[2] Correlatively, a decrease in the molecular volume by several Å^3 is usually characterized. Spin-crossover complexes can furthermore change their spin state upon the variation of a thermodynamic parameter such as temperature or pressure or by the application of a perturbation like an intense magnetic field[3] or light irradiation.[1] In the lat-

ter case, the process leading to the LS→HS conversion is reversible[4] and is called the LIESST effect (Light Induced Excited Spin State Trapping).[5] The relaxation from the light-induced metastable HS state to the thermodynamically stable LS state is attributed to a tunnel mechanism at very low temperature and to a much faster thermal activation over an energy barrier at higher temperature. Accordingly, the metastable HS state can be trapped at very low temperature. Recently, it has been shown that an elegant way to characterize the photomagnetic properties is to measure the T_{LIESST} temperature, which somewhat represents the temperature at which the metastable state relaxes quickly.[6,7] For weakly cooperative systems, the relaxation obeys single-exponential kinetics, whereas in the case of high cooperativity, the relaxation rate follows sigmoidal kinetics, ascribed to an autoaccelerated phenomenon owing to the HS→LS large molecular volume change and long-range elastic interactions in the solid.[8]

The structural aspects of spin-crossover complexes, and especially their relationship with respect to the spin transition characteristics, are nowadays raising a renewed interest. Direct correlations do exist between the distortion of the iron coordination octahedron and the features of the spin transition (e.g. T_{LIESST}).[9] Careful investigations of the structural modifications occurring during the thermal spin transition were reported in the literature and were mostly

[a] Laboratoire de Cristallographie et Modélisation des Matériaux Minéraux et Biologiques, LCM3B, UMR CNRS 7036, Nancy-Université
BP 239, 54506 Vandoeuvre-les-Nancy, France
Fax: +33-383406492
E-mail: claude.lecomte@lcm3b.uhp-nancy.fr
[b] Institut Laue Langevin
6 rue Jules Horowitz, BP 156, 38042 Grenoble Cedex 9, France
[c] ICMCB, CNRS, Université Bordeaux 1
87 avenue du Docteur Schweitzer, 33608 Pessac cedex, France

based on the comparison between the crystal structures in the HS state at room temperature and in the LS state at low temperature. Obviously, such studies suffer from thermal contraction effects, rendering a quantitative analysis quite meaningless if one wants to investigate fine structural details. In addition, atomic displacement parameters are not comparable between room temperature and low temperature; significant corrections to bond lengths would therefore also be required from libration motion.[10] The perturbation due to thermal contraction effects can be estimated, in a first approximation, by using isostructural materials which do not undergo the spin transition, e.g. by exchanging the central transition-metal ion.[11] A better strategy would take advantage of a hysteresis loop, if any, centred on the thermal spin transition, to derive the crystal structure in both the HS and LS states at identical temperature. For almost a decade, the crystal structures of light-induced metastable HS states have been reported for an increasing number of systems; they were derived from X-ray or neutron diffraction measurements performed at very low temperatures under light excitation.[12] These studies are possible thanks to the slowing of the HS to LS relaxation rate at very low temperature.[8] In some cases, a metastable HS state can also be trapped by rapid thermal quenching from room temperature to very low temperature: for example, the HS crystal structure of [Fe(PM–BiA)$_2$(NCS)$_2$] (PM = N-2′-pyridylmethylene and BiA = 4-aminobiphenyl) was determined at 30 K.[13] Following previous notations, the metastable HS state is denoted by HS-2 from this point onwards in this paper (HS-2q and HS-2p are used for the thermally quenched and photoinduced states, respectively); the HS state above the thermal transition is denoted by HS-1 (Figure 1). Finally, very recently, high-resolution X-ray diffraction measurements on the spin-crossover compounds [Fe(btr)$_2$(NCS)$_2$]·H$_2$O [btr = 4,4′-bis(1,2,4-triazole)] and [Fe(phen)$_2$(NCS)$_2$] (phen = 1,10-phenanthroline) have shown the possibility of the modelling of the electron-density distribution and the characterization of its redistribution upon spin transition, for instance, over the iron 3d atomic orbitals.[14–16] Whether the HS-2 states are identical within each other and how they compare to the HS-1 state are still controversial topics. In some cases, it has been proved that HS-2p and HS-2q are structurally different from HS-1 without any ambiguity, for instance in [Fe(abpt)$_2$-(N(CN)$_2$)$_2$],[17] leading to the concept of multimetastability.[18]

[Fe(btr)$_2$(NCS)$_2$]·H$_2$O is the archetype of highly cooperative spin-crossover compounds. It exhibits abrupt thermal spin transitions with a 21-K hysteresis loop ($T_{1/2\downarrow}$ = 123.5 K and $T_{1/2\uparrow}$ = 144.5 K). This complex crystallizes in the monoclinic space group $C2/c$ without any symmetry change at the thermal spin transition. The crystal structure consists of an Fe^{II} ion located in a slightly distorted FeN$_6$ centrosymmetric octahedral environment with four btr groups in the basal plane and two *trans* thiocyanate ligands in the apical directions (Figure 2). The btr group is a bidentate ligand leading to a bidimensional extended layer structure parallel to the bc plane. The NCS anions are directed
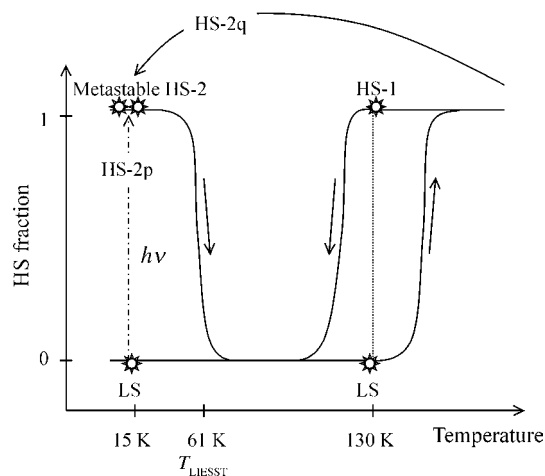

Figure 1. Schematic structural phase diagram (see text for the phase labelling).

away from the layers. The connection in the third direction is provided through van der Waals interactions and assisted by weak hydrogen bonds through a noncoordinated water molecule. On the basis of this specific polymeric layer structure, one might expect high cooperative interactions in the bc plane. The crystal structure was determined above and below the thermal transition at 293 K in the HS state[19] and at 104 K in the LS state.[20] The major structural modifications related to this transition are a shortening of the Fe–N bond lengths [$\Delta d_{\text{Fe–NCS}}$ = –0.175(4) Å, $\Delta d_{\text{Fe–N(btr)}}$ = –0.213(3) Å] and a reorientation of the NCS groups with a more linear Fe–N–C–S geometry in the LS state in parallel to a contraction of the unit cell by 4.8 % [ΔV = –91(9) Å^3]. This system has been the subject of various studies at the thermal spin transition. The hysteresis loop has been followed by magnetic measurements and Mössbauer spectroscopy.[19] The effect of metal dilution was analyzed in [Fe$_x$M$_{1-x}$(btr)$_2$(NCS)$_2$]·H$_2$O (M = Co, Ni) mixed systems, by calorimetric, magnetic and Mössbauer measurements;[21] these studies showed that metal dilution smoothes the transition curves. The first studies of the metastable HS state were performed through reflectivity and magnetic measurements on [Fe$_x$Co$_{1-x}$(btr)$_2$(NCS)$_2$]·H$_2$O derivatives;[22] the authors studied the LIESST relaxation and the LITH (Light Induced Thermal Hysteresis) loop under permanent irradiation at λ = 600 nm and 40 mW cm^{-2}. Finally, it has been shown that the HS ↔ LS transition is related to a domain nucleation, growth and coarsening process in the solid state, with an unprecedented light-induced structural reorganization.[20,23]

We report here a detailed structural analysis of [Fe(btr)$_2$-(NCS)$_2$]·H$_2$O in various spin states, HS-1, LS, HS-2q, HS-2p, by using X-ray diffraction measurements performed at two temperatures, 15 K and 130 K (Figure 1). The main goal of this study is the characterization of the structural reorganization related to the light-induced and thermally induced spin transitions independent of thermal contraction/expansion effects. Our structural findings are correlated to magnetic and spectroscopic results, which allows us
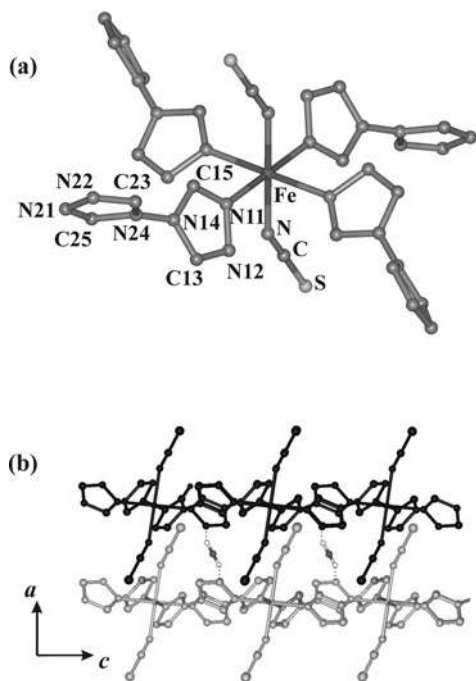
2

Figure 2. (a) Molecular structure of $[Fe(btr)_2(NCS)_2] \cdot H_2O$ in the HS-2q state at 15 K. (b) View of the layer stacking along the a axis. Hydrogen atoms of the btr groups are omitted for clarity.

to define the appropriate experimental conditions for the photocrystallographic measurements. We must emphasize that, for consistency, single crystals of similar quality and size were used in all the experiments reported here.

Results and Discussion

Optical Spectroscopy

$[Fe(btr)_2(NCS)_2] \cdot H_2O$ exhibits thermochromic effects associated with the HS–LS transition, from colourless at room temperature to pink at low temperature. The change in the diffuse absorption spectrum as a function of temperature is given in Figure 3. On decreasing the temperature from 160 K to 100 K and passing through the thermal HS-to-LS transition, the absorption band with a maximum intensity at 550 nm ($18200\ cm^{-1}$) increases in intensity. This band is characteristic of the LS state and is attributed to the spin-allowed $^1A_1 \rightarrow {}^1T_1$ transition, according to the Tanabe–Sugano diagram for Fe^{II} (d^6) in an octahedral ligand field. In parallel, the band with a maximum intensity at 875 nm ($11400\ cm^{-1}$), characteristic of the HS state and corresponding to the $^5T_2 \rightarrow {}^5E$ transition, decreases in intensity. Below nearly 75 K, the 550-nm absorption band is gradually attenuated to a minimum value at 10 K owing to the partial LS-to-HS phototransformation under the probing white beam ("LITH down" in Figure 3). On further increasing the temperature to 100 K, first the 550-nm absorption band remains almost constant and in a second step increases in intensity, corresponding to the relaxation from HS to LS ("LITH up" in Figure 3). Finally, from 100 K to 160 K, the

LS-to-HS thermal transition occurs, the 550-nm absorption band is attenuated and recovers its initial value. In such diffuse absorption measurements, the intensity ratio of the $^5T_2 \rightarrow {}^5E$ and $^1A_1 \rightarrow {}^1T_1$ bands should not be taken too strictly, because they may change owing to powder sample texture effects; therefore, they cannot be directly compared to single-crystal absorption spectra. In addition, a slight bleaching of the powder sample, resulting possibly from surface dehydration, has been noticed at the end of the measurement, which could alter the intensity of the $^5T_2 \rightarrow {}^5E$ band. It is indeed known that dehydrated $[Fe(btr)_2(NCS)_2] \cdot H_2O$ loses its spin-transition behaviour and is a HS system.
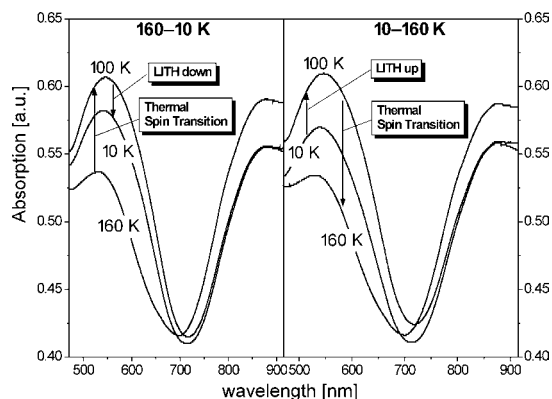

Figure 3. Diffuse absorption spectra as a function of temperature in the cooling (160–10 K) and warming (10–160 K) modes. The 10-K spectrum corresponds to the photostationary state under the experimental conditions of the reflectivity measurements.

This 550-nm absorption band displays a high contrast depending on the spin state. The diffuse reflected intensity vs. temperature at the wavelength λ = 532 nm was thus investigated in more detail and is given in Figure 4. The thermal hysteresis loop is well defined with $T_{1/2\downarrow}$ = 123 K and $T_{1/2\uparrow}$ = 144 K, in perfect agreement with magnetic and crystallographic results.[19,20] On decreasing the temperature from 75 to 10 K, we observe an increase in the reflectivity signal, corresponding to partial LS-to-HS conversion induced by the probing white light. Then, as the temperature is increased further, the signal presents a constant plateau till nearly 62 K, at which the LS value is recovered. This loop, defined below 75 K, corresponds to the light-induced thermal hysteresis phenomenon (LITH),[24] already discussed by Desaix et al.,[22] and clearly confirms the existence of a photoinduced instability for $[Fe(btr)_2(NCS)_2] \cdot H_2O$. By comparison of the reflectivity value at the photostationary state (0.43) with those obtained for the purely LS (0.39) and purely HS (0.46) states, we can estimate a surface photoconversion, γ_{HS}, of nearly 0.5 at saturation.

The spin selectivity of the bands centred at 550 nm and 875 nm indicates that they correspond to the optimum laser wavelengths for inducing the LS-to-HS-2 (LIESST) and HS-2-to-LS (reverse LIESST) conversions, respectively. This information is crucial for defining the excitation conditions for the photocrystallographic measurements.
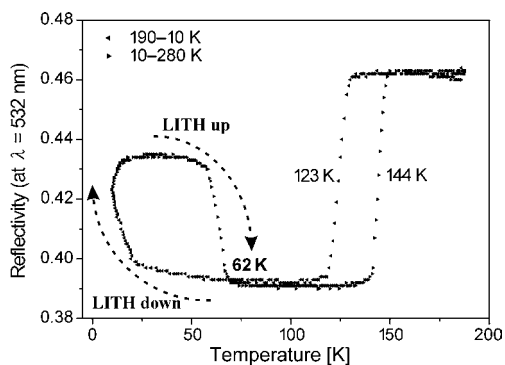
Figure 4. Reflectivity measurements as a function of temperature at λ = 532 nm in the cooling (190–10 K) and warming (10–280 K) modes: $T_{1/2\downarrow}$ = 123 K, $T_{1/2\uparrow}$ = 144 K.

Magnetic Behaviour of the Light-Induced and Thermally Induced Metastable States

The magnetic properties as a function of temperature and light irradiation were investigated by using different measurement procedures. For the first measurement (Figure 5a), the sample was rapidly quenched to 10 K in the HS-2q state. Then, the temperature was raised in the dark; $\chi_M T$ initially increases slightly, as a result of zero-field splitting of the quintet HS-2 state, before reaching a plateau and then sharply falls off to 0 cm³ K mol⁻¹ at 61 K, indicating a complete relaxation of the molecular species into the LS state. After the relaxation, the thermal transitions were recorded in the warming and cooling modes and are consistent with literature results:[19] very abrupt and complete transitions at $T_{1/2\downarrow}$ = 123.5 K and $T_{1/2\uparrow}$ = 144.5 K. The $\chi_M T$ value at low temperature on the plateau is nearly identical (3.5 cm³ K mol⁻¹) to that observed at high temperature in the HS-1 state, suggesting that the quenched state corresponds to almost γ_{HS} = 1. The T_{TIESST} (Thermally Induced Excited Spin State Trapping) value is estimated at 61 K, and the HS-2-to-LS relaxation at this temperature is as abrupt as those for the thermal transitions. These magnetic measurements prove without any ambiguity that it is possible to quench [Fe(btr)$_2$(NCS)$_2$]·H$_2$O single-crystal samples in the HS-2q state.

For the second measurement (Figure 5b), the sample was cooled gradually from room temperature (HS-1 state) to 10 K (LS state) and then irradiated with a laser at λ = 514 nm (P = 5 mW cm⁻²) to promote the HS-2p state. The $\chi_M T$ value rose up to 0.63 cm³ K mol⁻¹ after a 15-h continuous irradiation, which indicates partial LS-to-HS-2p photoconversion. By comparison with the $\chi_M T$ value obtained at 160 K for the HS-1 state (3.0 cm³ K mol⁻¹), a photoconversion of about 21% is estimated. On increasing the temperature in the dark, the HS-to-LS relaxation is observed at T = 61 K. Under 60-mW cm⁻² excitation with green light of 550 nm wavelength at T = 10 K, Morscheidt et al.[25] also induced a partial conversion of at most 20% HS-2.
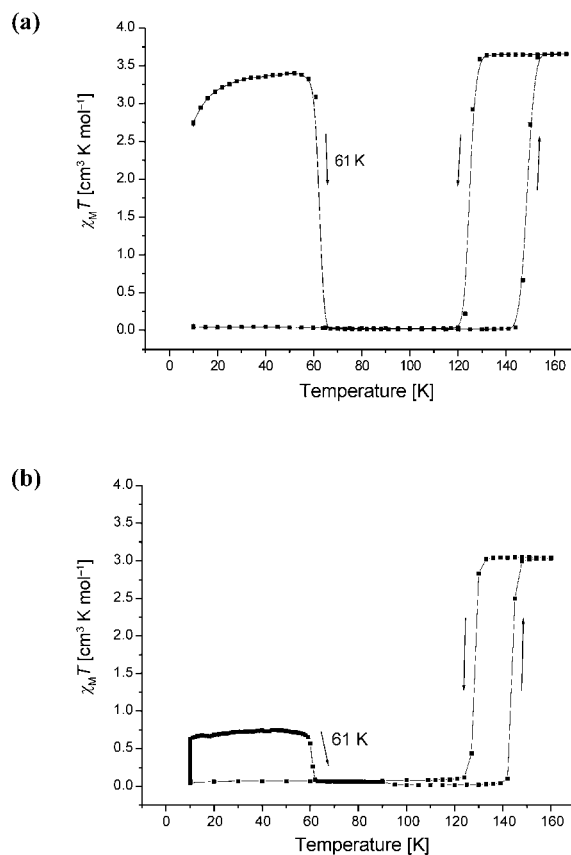

Figure 5. Temperature dependence of $\chi_M T$ for (a) the thermally quenched sample and (b) the photoinduced sample.

Finally, the photoexcitation and relaxation kinetics were derived. The magnetic signal was recorded during a 23-h continuous irradiation at 10 K at λ = 514 nm (Figure 6a). It clearly shows a nonlinear sigmoidal behaviour, which has been attributed to a competition between photoexcitation and relaxation by Enachescu et al. for [Fe$_x$M$_{1-x}$(btr)$_2$-(NCS)$_2$]·H$_2$O derivatives (M = Ni, Co, Zn).[26] This is the basis for the light-induced instability phenomenon. After saturation of the magnetic signal at 0.89 cm³ K mol⁻¹, the excitation light was turned off, and the magnetic signal was monitored in the dark. The negligible change in the signal in the dark, although a slight negative trend is noticeable, confirms the high stability of the HS-2 state at T = 10 K, in the tunnel relaxation regime. The reverse-LIESST effect was then induced by using an excitation wavelength corresponding to the ⁵T$_2$→⁵E transition at λ = 830 nm (following the optical reflectivity results); the irradiance was set to 5 mW cm⁻². The sudden change in the slope and the continuous decrease in the magnetic signal therefore confirm the reversibility of the light-induced LS–HS conversion for $T < T_{LIESST}$. The molar magnetic susceptibility of the HS-2 state at 10 K after thermal trapping was also monitored as a function of time and converted to γ_{HS} (Figure 6b) in order to calibrate the 15-K photocrystallographic measurements. The relaxation kinetics is very slow at this temperature, which is well below T_{LIESST} and T_{TIESST}, and corresponds to the tunnel relaxation regime.
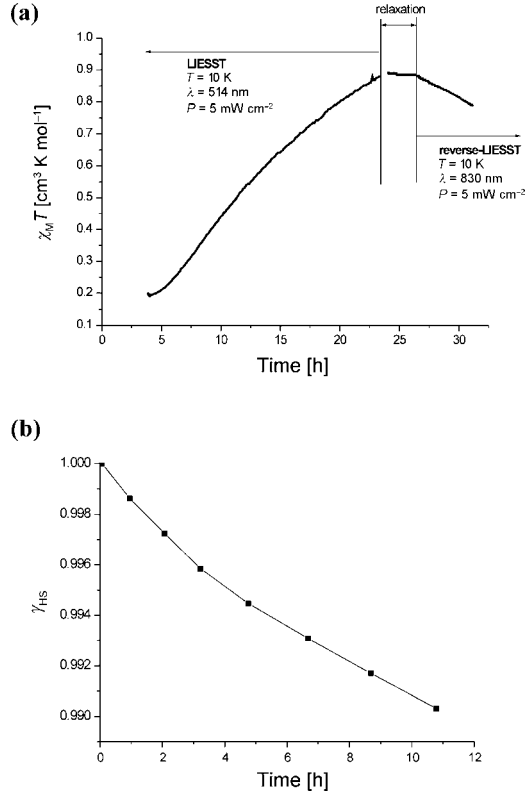
(a)

(b)

Figure 6. (a) Time dependence of $\chi_M T$ during LS→HS photoexcitation (LIESST) and HS→LS photorelaxation (reverse-LIESST) at 10 K. (b) Relaxation kinetics of the quenched metastable HS state in the dark at 10 K, derived from susceptibility measurements as a function of time.

All together, these magnetic results, in addition to the previous optical properties, are mandatory for the choice of appropriate experimental conditions for the photocrystallographic measurements (temperature, excitation wavelength and duration). They indeed confirm the possibility for a careful X-ray diffraction measurement on the HS-2q and HS-2p states at very low temperature ($T \approx 10$ K), as the necessary requirements are met: possible photoconversion, efficient thermal quenching, high relaxation T_{LIESST} and T_{TIESST} temperatures and an almost negligible relaxation rate at sufficiently low temperature (10 K).

Thermal Expansion Analysis

The lattice constants of [Fe(btr)$_2$(NCS)$_2$]·H$_2$O were derived from single-crystal X-ray diffraction as a function of temperature (15 K < T < 270 K) in all the different spin states and are reported in Figure 7. From room temperature to 124 K, in the HS-1 state, the a and b cell axes contract linearly, whereas the c axis slightly expands in a linear fashion, leading to a thermal contraction of the unit cell volume. Upon passing the thermal spin transition at $T_{1/2\downarrow}$ = 124 K, the lattice constants change abruptly, giving a cell volume variation, ΔV_{HL}, of –91 Å^3 (5%). In the LS state (15 K < T < 144 K), a contraction of the a and b axes and an expansion of the c axis are observed. Remarkably, the

lattice parameters in the metastable HS-2 states are in almost perfect linear continuity to those of the HS-1 state. At 15 K, the cell volume expansion from LS to HS-2, ΔV_{HL} = +91 Å^3, exactly matches the volume variation at the thermal transition.
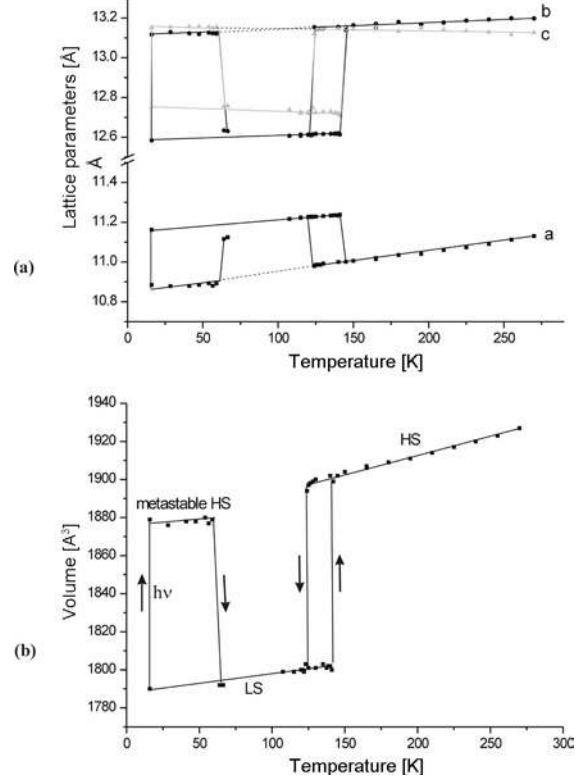

(a)

(b)

Figure 7. (a) Unit cell parameters and (b) unit cell volume as a function of temperature (15–270 K).

The temperature dependence of the lattice constants was further analyzed by using the formalism of the lattice expansion model.[27] This model, which is based on the assumption of a direct proportionality between the HS–LS cell volume change and γ_{HS}, was efficiently used to describe the behaviour of several spin-crossover materials such as [Fe(mtz)$_6$]·(BF$_4$)$_2$ and [Fe(ptz)$_6$]·(BF$_4$)$_2$.[28,29] In the generalized form of this model, a vector, $\mathbf{X}(T)$, is given by Equation (1):

$$\mathbf{X}(T) = \{\mathbf{1} + \boldsymbol{\alpha}T + \boldsymbol{\varepsilon}\gamma_{\text{HS}}(T)\}\mathbf{X}(T=0) \tag{1}$$

In Equation (1), $\boldsymbol{\alpha}$ is related to the thermal expansion of the crystal lattice, whereas $\boldsymbol{\varepsilon}$ describes the spontaneous strain (deformation) of the crystal lattice upon LS–HS transition. The thermal expansion of a crystal lattice is well described by the Grüneisen approximation, including anharmonicity contributions. The free energy of the crystal lattice is parameterized by its bulk modulus, the vibration energy of the phonons and the Grüneisen constant.[30] In a first approximation, $\boldsymbol{\alpha}$ is assumed to be the same in the HS and LS states, which is usually quantitatively sufficient for spin-crossover materials whose crystal structure consists of individual molecular entities.

The lattice parameters were fitted by the least-squares method to linear functions, whose coefficients exhibit significant spin dependencies (Table 1). Accordingly, we anticipate that the assumption that the thermal-expansion tensor, **α**, is the same for both spin states is hardly fulfilled in the case of [Fe(btr)$_2$(NCS)$_2$]·H$_2$O, because of its particular 2D polymeric crystal structure. Indeed, different phonon vibration energies might be expected on changing from the LS to the HS state. In such a case, a more general expression of the lattice expansion model given by Equation (1), including spin-dependent thermal-expansion tensors **α**$_{HS}$ and **α**$_{LS}$, is required [Equation (2)]:

$$\mathbf{X}(T) = \left[1 + \left\{ \gamma_{HS}(T)\boldsymbol{\alpha}_{HS} + [1 - \gamma_{HS}(T)]\boldsymbol{\alpha}_{LS} \right\} T + \boldsymbol{\varepsilon}\gamma_{HS}(T) \right] \mathbf{X}\ (T=0) \tag{2}$$

Table 1. Results of the least-squares fit of the lattice parameters as a function of temperature using linear functions $\mathbf{X}(T) = \mathbf{X}(0) + \boldsymbol{\alpha}_L T$.

Parameter	Spin state	Fitted functions
a	HS	$10.857(3) + 9.9(2) \times 10^{-4}\ T$
	LS	$11.157(1) + 5.7(1) \times 10^{-4}\ T$
b	HS	$13.106(4) + 3.4(3) \times 10^{-4}\ T$
	LS	$12.581(2) + 2.6(2) \times 10^{-4}\ T$
c	HS	$13.153(5) - 7(3) \times 10^{-5}\ T$
	LS	$12.76(1) - 2.6(7) \times 10^{-4}\ T$
β	HS	$90.74(4) + 3.5(36) \times 10^{-3}\ T$
	LS	$92.37(3)$

By using $\gamma_{HS}(T)$ derived from the magnetic measurements, the elements of the tensors **α**$_{HS}$, **α**$_{LS}$ and **ε** in Equation (2) were fitted to the measured values of the lattice parameters vs. temperature through a Monte Carlo algorithm, until the minimum of the agreement function $R = \Sigma[x_{obs}(T) - x_{calc}(T)]^2/\Sigma[x_{obs}(T)]^2$ was reached. Results of the fit are given in Table 2. The orthonormal coordinate system attached to the crystal was defined as conventional in the monoclinic system: $e_2//b$, $e_3//c$ and $e_1//a*$.

The elements of the **α**$_{HS}$ and **α**$_{LS}$ tensors clearly indicate a similar behaviour with nonetheless some specific discrepancies. In both spin states, the largest eigenvalue corre-

Table 2. Coefficients a_{ij} and eigenvalues a_{ij}^0 of the thermal-expansion tensors (**α**$_{LS}$, **α**$_{HS}$) and coefficients ε_{ij} and eigenvalues ε_{ij}^0 of the spontaneous-strain tensor (**ε**).

	a_{11} [10^{-5} K^{-1}]	a_{22} [10^{-5} K^{-1}]	a_{33} [10^{-5} K^{-1}]	a_{13} [10^{-5} K^{-1}]
α$_{HS}$	8.86(7)	2.62(1)	–0.58(1)	–3.00(8)
α$_{LS}$	5.05(3)	2.08(1)	–2.08(2)	–0.043(1)
	a_{11}^0 [10^{-5} K^{-1}]	a_{22}^0 [10^{-5} K^{-1}]	a_{33}^0 [10^{-5} K^{-1}]	Tr(**α**) [10^{-5} K^{-1}]
α$_{HS}^0$	9.73(7)	2.62(1)	–1.43(1)	10.92(9)
α$_{LS}^0$	5.05(3)	2.08(1)	–2.08(2)	5.05(6)
	ε_{11} [10^{-2}]	ε_{22} [10^{-2}]	ε_{33} [10^{-2}]	ε_{13} [10^{-2}]
ε	–2.62(1)	4.17(1)	3.11(1)	1.46(1)
	ε_{11}^0 [10^{-2}]	ε_{22}^0 [10^{-2}]	ε_{33}^0 [10^{-2}]	Tr(**ε**) [10^{-2}]
ε^0	–2.97(1)	4.17(1)	3.46(1)	4.66(3)

sponds to an eigendirection almost along the crystallographic a axis, that is to say perpendicular to the structural layers, as can be seen in Figure 8. The coefficients a_{22}^0 and a_{33}^0 correspond to two mutually perpendicular directions roughly parallel to the structural layers. The interlayer region is therefore the most affected by temperature ($a_{11}^0 > a_{22}^0$, a_{33}^0); the corresponding thermal contraction is furthermore almost twice as large in the HS state [$a_{11}^0 = 9.73(7) \times 10^{-5}$ K^{-1}] as that in the LS state [$a_{11}^0 = 5.05(3) \times 10^{-5}$ K^{-1}]. Correlatively, the overall thermal volume contraction, approximated by the trace of the **α** tensor [Tr(**α**) = $a_{11}^0 + a_{22}^0 + a_{33}^0$], is also twice as large in the HS state. This behaviour correlates to a slight reduction of the hydrogen-bond strength, which is responsible for the interlayer connection, in the HS state with an increase in the Ow···N12 distances [$d_{Ow···N12}$(LS) = 3.026(3) Å and $d_{Ow···N12}$(HS) = 3.065(1) Å at 130 K for instance]. In both spin states, the thermal volume contraction is much lower than that observed for molecular spin-crossover systems {Tr(**α**) = 26×10^{-5} K^{-1} at 298 K in the HS state for [Fe(PM-BiA)$_2$(NCS)$_2$] for instance},[11] due to the lower sensitivity to deformation of the crystal lattice of [Fe(btr)$_2$(NCS)$_2$]·H$_2$O. This is expected on the basis of its polymeric crystal structure.
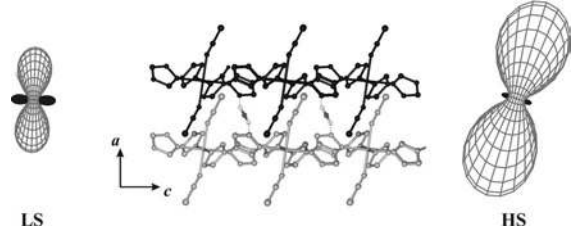

Figure 8. Representation of the thermal-expansion tensor in the HS and LS states oriented with respect to the layer crystal structure. Positive thermal expansion is displayed in light grey, negative in black.

The spontaneous strain at the HS–LS transition is also highly anisotropic, with a negative contribution along the crystallographic a axis and positive values along the b and c axes. The HS–LS transition correlates therefore to an increase in the interlayer spacing and an overall contraction parallel to the layers. The former aspect is related to a reorientation of the NCS group with a more linear Fe–N–C–S geometry in the LS state (see below), whereas the contraction within the layer is connected to the abrupt Fe–N bond shortening at the transition. Note that **ε** was fitted on the whole temperature range, and it therefore assumes an identical spontaneous strain at the thermal and light-induced transitions.

Similarities between the HS-2q and HS-2p Structures

The lattice parameters exhibit systematic positive differences from HS-2p to HS-2q: Δa = 0.031(2) Å, Δb = 0.049(2) Å, Δc = 0.015(2) Å [ΔV = 14.4(5) Å^3]. This positive

volume discrepancy would suggest that HS-2p corresponds to an incomplete metastable HS-2 state with some residual LS species. The comparative structural characteristics of the FeN_6 octahedron are given in Table 3. On the whole, the mean-square atomic position deviation, *mfa*, is only 0.0125 Å between these two metastable HS-2 crystal structures, as calculated by mapping the structures of the Fe(btr)$_4$-(NCS)$_2$ fragment with KPLOT,[31] including only non-hydrogen atoms. It is worth noting that the bond lengths are systematically more precise and larger in the HS-2q state than in HS-2p, but the differences for the Fe–N bonds are within 2σ. The angular deformation of the FeN_6 octahedron, defined as the sum of the deviations from 90° of the 12 *cis* N–Fe–N angles in the coordination sphere,[2] shows some differences: Σ_{HS-2q} = 15.6(4)° and Σ_{HS-2p} = 18(2)°. The differences between HS-2p to HS-2q in the btr bond lengths and angles are in the range of the experimental uncertainty, except for the N14–N24, N22–C23 and N21–C25 bonds which are at the limit of the statistical significance. The geometry of the NCS ligand is also very similar, with bond lengths, *d*(N–C), of 1.179(1) and 1.174(8) Å and *d*(C–S) values of 1.634(1) and 1.631(6) Å for the HS-2q and HS-2p states, respectively. The interlayer Ow–Hw···N12 hydrogen-bond contacts present the same structural characteristics, with Ow···N12 distances of 3.044(2) and 3.036(7) Å for the HS-2q and HS-2p states, respectively, correlated to a slight displacement of the water molecule [Δd(Ow) = 0.009(3) Å].

Table 3. Selected structural characteristics in the various spin states. The octahedron volume V_p was calculated with IVTON.[44].

Bond length [Å]	15 K			130 K	
	LS	HS-2q	HS-2p	LS	HS-1
Fe–N$_{NCS}$	1.9498(5)	2.131(1)	2.129(4)	1.949(2)	2.1283(7)
Fe–N11	1.9730(5)	2.171(1)	2.166(6)	1.976(1)	2.1786(5)
Fe–N21	1.9685(5)	2.165(1)	2.154(5)	1.968(1)	2.1710(5)
N–C	1.1753(7)	1.179(1)	1.174(8)	1.169(2)	1.173(1)
C–S	1.6405(5)	1.634(1)	1.631(6)	1.640(2)	1.6254(8)
Ow···N12	3.0247(7)	3.044(2)	3.036(7)	3.026(3)	3.065(1)
Angle [°]					
N–Fe–N11	90.17(2)	90.71(4)	90.9(2)	90.12(6)	90.72(3)
N–Fe–N21	92.32(2)	92.34(3)	92.3(2)	92.24(6)	92.28(2)
N11–Fe–N21	88.79(2)	89.14(4)	88.6(2)	88.77(6)	89.16(3)
Fe–N–C	162.79(4)	149.46(8)	149.0(5)	163.1(1)	150.66(6)
Σ [°]	14.8(2)	15.6(4)	18(2)	14.4(7)	15.4(3)
V_p [Å^3]	10.09(1)	13.34(1)	13.2(1)	10.10(1)	13.41(1)

According to the structural arguments presented here, we cannot firmly confirm or reject the hypothesis that HS-2q and HS-2p correspond to a unique phase in the case of [Fe(btr)$_2$(NCS)$_2$]·H$_2$O.

LS→HS-2q Structural Modifications at 15 K

Figure 9 presents a superposition of the molecular structures in the LS and HS-2q states at 15 K. The mean-square atomic position deviation,[31] *mfa*, which in this case gives insight into the mean magnitude of the LS-to-HS-2q atomic displacement, is 0.272 Å (Table 4). This value is very similar

for the LS-to-HS-2p transition (*mfa* = 0.270 Å). Upon the LS-to-HS-2q spin-state change, the Fe–N coordination bonds expand by Δd(Fe–N$_{NCS}$) = 0.181(2) Å, Δd(Fe–N11) = 0.198(2) Å and Δd(Fe–N21) = 0.196(2) Å. The deformation of the FeN_6 octahedron is slightly lower in the LS state [Σ_{LS} = 14.8(2)°] than in the HS-2q phase [Σ_{HS-2q} = 15.6(4)°], which is the usual trend for such iron(II) compounds. However, these deformations are much less severe than those for other Fe(L)$_2$(NCS)$_2$ spin-transition complexes whose Σ_{HS} values are typically around 70°.[2] The FeN_6 octahedron volume changes by ΔV_p = +3.25(2) Å^3, which accounts for only 14% of the total unit cell volume variation (ΔV_{cell} = +92 Å^3), since there are four iron octahedrons per unit cell. During the spin-state change, the NCS ligand, in the *trans* position, undergoes a reorientation by $\Delta\theta_{LH}$ = –13.3(1)°, the Fe–N–C angle being closer to 180° in the LS state than in the HS-2q state. As discussed above, this NCS reorientation is correlated to the expansion of the crystallographic *a* axis, which increases the interlayer spacing, and therefore is the main contribution to ΔV_{cell}. As for the btr ligand, the variations in bond length and angle are
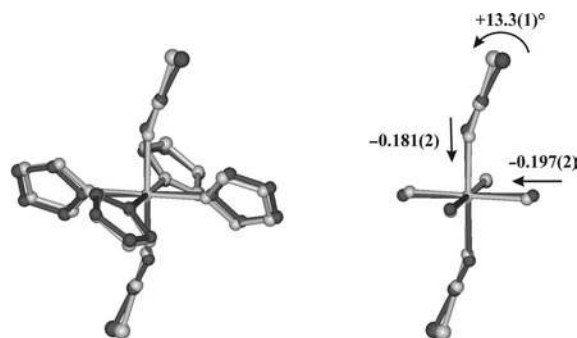

Figure 9. Superposition of the molecular structures in the LS state (grey) and the HS-2q state (black) at 15 K.

Table 4. Geometrical reorganization of the FeN_6 octahedron upon various spin-state changes. *mfa* is the mean-square atomic position deviation, given by $mfa = (\sum_{i=1}^{n} S_i^2/n)^{1/2}$, where the S_i are the distances [Å] between corresponding pairs of atoms in the two structures. *mfa* was calculated by using KPLOT.[31]

Bond length [Å]	LS→HS-2p (15 K)	LS→HS-2q (15 K)	LS→HS-1 (130 K)
Fe–N	+0.179(5)	+0.181(2)	+0.179(2)
Fe–N11	+0.193(7)	+0.198(2)	+0.202(2)
Fe–N21	+0.185(6)	+0.196(2)	+0.203(2)
N–C–S	–0.01(1)	–0.002(3)	–0.011(6)
Ow···N12	+0.011(8)	+0.019(3)	+0.039(4)
Angle [°]			
N–Fe–N11	+0.7(2)	+0.54(6)	+0.60(9)
N–Fe–N21	0.0(2)	+0.02(5)	+0.04(8)
N11–Fe–N21	–0.2(2)	–0.34(6)	–0.39(8)
Fe–N–C	–13.8(5)	–13.3(1)	–12.5(2)
$\Delta\Sigma$ [°]	+3(2)	+0.8(6)	+1(1)
ΔV_p [Å^3]	+3.1(1)	+3.25(2)	+3.31(2)
mfa [Å]	0.270	0.272	0.266

within the experimental uncertainty, whereas the dihedral angle between the triazole rings increases significantly from 84.81(3)° to 88.20(6)°. Finally, we note a displacement of the water molecule along the crystallographic b direction [$\Delta d(\text{Ow})_{\text{HL}} = -0.236(1)$ Å] resulting in a small increase in the interlayer Ow···N12 contacts by 0.019(3) Å.

LS→HS-1 Structural Reorganization at 130 K

Upon the LS-to-HS-1 spin-state change at 130 K, the mean-square atomic position deviation is 0.266 Å, which is marginally lower than that calculated for the LS-to-HS-2q transition. As a matter of fact, the 130 K HS and 15 K HS-2q states are closely related to each other ($mfa = 0.0317$ Å); this criterion is even lower for the corresponding LS structures ($mfa = 0.0155$ Å). The coordination bonds expand by $\Delta d(\text{Fe–N}_{\text{NCS}}) = 0.179(2)$ Å, $\Delta d(\text{Fe–N11}) = 0.202(2)$ Å and $\Delta d(\text{Fe–N21}) = 0.203(2)$ Å, which are within the σ values calculated for the LS-to-HS-2q spin-state change. As for the latter, the angular distortion of the FeN$_6$ octahedron is smaller in the LS state [$\Sigma_{\text{LS}} = 14.4(7)°$] than in the HS-1 one [$\Sigma_{\text{HS-1}} = 15.4(3)°$]. The FeN$_6$ octahedron volume changes by $\Delta V_{\text{p}} = +3.31(2)$ Å^3, which accounts for nearly 13% of the unit cell volume change ($\Delta V_{\text{cell}} = 99$ Å^3), similar to the LS-to-HS-2q spin-state change. The bond length variations of the btr ligand between the two spin states are within the uncertainty, except for the bonds C13–N14 and C23–N24, which are slightly longer in the LS state. The dihedral angle between the triazole ring planes has the same values as at 15 K [84.8(1)° and 88.32(4)° in the LS and HS-1 states, respectively]. Again, as for the LS-to-HS-2q transition at 15 K, we observe a reorientation of the NCS by $\Delta\theta_{\text{LH}} = -12.5(2)°$. Finally, we note a 0.039(4)-Å increase in the intermolecular Ow···N12 contact in the HS-1 state with respect to the LS state. The displacement of the water molecules along the crystallographic b direction is in this case $\Delta d(\text{Ow})_{\text{HL}} = -0.255(1)$ Å. As a conclusion, we can claim that the LS→HS-2q and LS→HS-1 transitions lead to almost identical structural modifications.

Thermal Motion Analysis

The importance of molecular vibrations in the spin conversion phenomenon was first recognized by Sorai and Seki on the basis of calorimetric measurements; they indeed revealed that the spin transition is an entropy-driven process.[32] If we look in general at spin-crossover materials, ΔS_{LH} typically amounts to about 50 J K^{-1} mol^{-1}, of which the vibrational contribution to the molar entropy accounts merely for 60–70%, while the electronic (spin multiplicity) entropy represents only 13.4 J K^{-1} mol^{-1} in the case of Fe$^{\text{II}}$ spin-crossover complexes. It is generally assumed that the major contributions to the vibrational entropy results from the 15 intramolecular normal modes of the regular FeN$_6$ octahedron and predominantly from the Fe–N stretching modes. Detailed IR and Raman spectroscopic measurements as well as nuclear inelastic scattering results, coupled

to ab initio DFT calculations on isolated molecules, indicate, on the other hand, that some external (phonon) modes might also contribute significantly to the vibrational entropy.[33] However, a comprehensive knowledge of the importance of these phonon modes is still missing. Several models for spin crossover account explicitly for the role of vibrations, through a reduced number of empirical parameters such as the HS and LS Debye temperatures [$\Theta_{\text{D}}(\text{HS})$ and $\Theta_{\text{D}}(\text{LS})$, Zimmerman and König model[34]] or the effective HS and LS degeneracies of electro-vibrational origin (ω_{HS} and ω_{LS} in the two-level Ising-like model introduced by Bousseksou et al.[35]).

Literature results indicate that for the title [Fe(btr)$_2$(NCS)$_2$]·H$_2$O complex, ΔS_{LH} is as high as 76 J K^{-1} mol^{-1}.[21a] On the basis of its specific extended layer structure, the large cell volume change and the structural modifications at the spin transitions, large modifications of the atomic vibration amplitudes are expected as well. For cyanide-bridged iron(II) spin-crossover complexes, which exhibit a polymeric crystal structure, it has been suggested from Raman measurements that the contribution from intermolecular vibration to the total entropy might be non-negligible.[36] This is most probably related to the strong cooperativity induced by the extended polymeric structure. For similar reasons, lattice vibrational modes might also play an important role in [Fe(btr)$_2$(NCS)$_2$]·H$_2$O. We have derived here the crystal structure in both spin states at two temperatures (15 K and 130 K), which affords the possibility to characterize the difference in vibrational behaviour (vibration modes and amplitudes) between HS and LS. The atomic vibration amplitudes, described through the atomic $\mathbf{U}_{ij}$ tensor in a conventional structural analysis (like the one performed here), consist of additive contributions from intramolecular vibration modes of high frequency and lattice vibrations (phonons) of lower frequency. For the thermal transition, the atomic displacement tensors were derived from the present structural analysis, whereas for the 15 K case, the atomic displacement tensors (for LS and HS-2q) were derived from the more accurate multipolar model of the electron density previously published.[16] In the latter, thermal vibrations are decorrelated from aspherical electron-density features. Recent experimental and theoretical investigations include the intramolecular normal modes of the regular FeN$_6$ octahedron as well as the ligand vibration modes through a multicoordinate approach.[33] We will rather follow here a simpler single-coordinate procedure.

Upon LS-to-HS state change (LS→HS-1 and LS→HS-2), a systematic enhancement in equivalent isotropic displacement parameters is observed, as shown in Table 5 and illustrated in Figure 10. The most striking feature is a similar trend from atom to atom at the two temperatures, the increase being nevertheless higher in almost all cases at 130 K. In the case of sulfur, the increase is much larger at 130 K than for all the other atoms and seems suspicious; it is most probably related to some disordering effects, which can not be resolved in the crystal structure analysis but are taken into account in the corresponding atomic displacement parameters. The systematic LS-to-HS increase in

Table 5. Equivalent isotropic displacement parameters, U_{equ}, [Å^2].

| | 15 K | | | 130 K | | |
	LS	HS-2q	ΔU_{equ} (LS→HS-2q)	LS	HS-1	ΔU_{equ} (LS→HS-1)
Fe	0.00414(2)	0.00459(5)	0.00045(7)	0.00925(8)	0.00870(2)	−0.0005(1)
N	0.00700(7)	0.0094(2)	0.0024(3)	0.0124(3)	0.01634(9)	0.0039(4)
C	0.00727(8)	0.0084(2)	0.0011(3)	0.0136(3)	0.01504(9)	0.0014(4)
S	0.00941(2)	0.0115(1)	0.0021(1)	0.0241(1)	0.03590(7)	0.0118(2)
N11	0.00587(7)	0.0075(2)	0.0016(3)	0.0105(2)	0.01321(8)	0.0027(3)
N12	0.00716(7)	0.0087(1)	0.0015(2)	0.0137(3)	0.01650(9)	0.0028(4)
C13	0.00734(8)	0.0091(2)	0.0018(3)	0.0147(3)	0.0172(1)	0.0025(4)
C15	0.00652(8)	0.0076(2)	0.0011(3)	0.0122(3)	0.01337(9)	0.0012(4)
N14	0.00613(7)	0.0070(2)	0.0009(3)	0.0116(2)	0.01281(8)	0.0012(3)
N24	0.00611(7)	0.0069(2)	0.0008(3)	0.0111(2)	0.01215(7)	0.0010(3)
N21	0.00592(7)	0.0068(2)	0.0009(3)	0.0102(2)	0.01199(7)	0.0018(3)
N22	0.00686(7)	0.0077(2)	0.0008(3)	0.0130(3)	0.01363(8)	0.0006(4)
C23	0.00711(8)	0.0077(2)	0.0006(3)	0.0138(3)	0.01404(9)	0.0002(4)
C25	0.00676(8)	0.0076(2)	0.0008(3)	0.0126(3)	0.01352(9)	0.0009(4)

atomic displacement amplitudes can be directly related to the spin transition and indicates vibration modes of globally larger amplitudes in the HS state; it can not be attributed to a population of higher-energy vibrational levels since measurements have been performed at rigorously the same temperature. This behaviour can be pictured by a mean potential well that is globally broader in the HS state (inset in Figure 10).
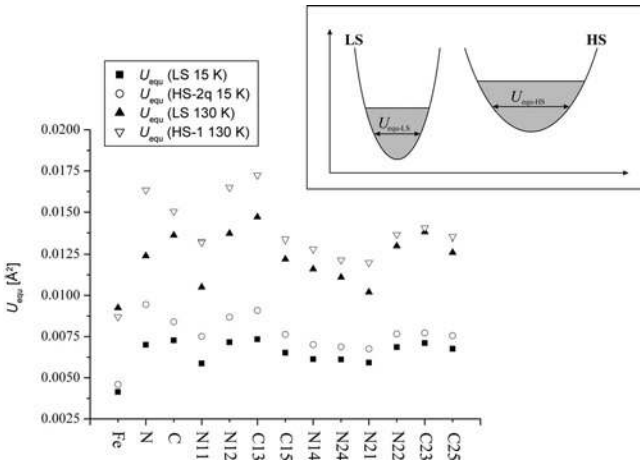

Figure 10. Equivalent isotropic displacement parameters U_{equ} [U_{equ} = $1/3(U_{11} + U_{22} + U_{33})$]. The S atom has been omitted as it is possibly affected by some disordering effects (see text). Inset: schematic representation of the mean HS and LS vibrational potential wells.

The inspection of the anisotropic displacement parameters allows us to proceed further. Figure 11 displays the difference mean-square surfaces [$U_{HS} − U_{LS}$] at 15 K and 130 K; it is evident that similar features are present at both temperatures. First of all, the atomic displacement amplitudes are systematically higher in the HS state with respect to the LS state, as discussed above. In the case of sulfur, the thermal motion is higher in the direction perpendicular to the NCS axis in the HS state, therefore characterizing a higher bending vibration of the NCS group together with a possible static disorder of the sulfur atom. The difference for btr also exhibits a systematic trend, the thermal motion

being higher in the direction perpendicular to each triazole ring for all atoms. The fact that all btr atoms behave collectively confirms that this behaviour is due to higher vibration amplitudes of external (lattice) modes in the HS state and is indeed related to the spin-state change.
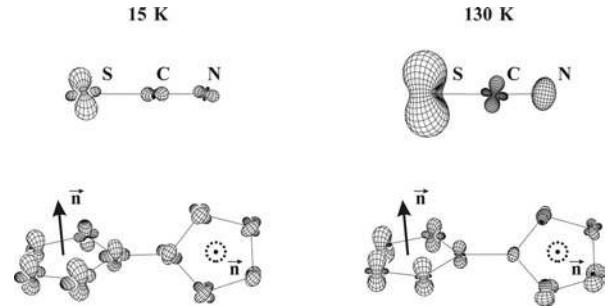

Figure 11. Difference mean-square surfaces [$U_{HS} − U_{LS}$] calculated by using PEANUT.[43] Positive surfaces are in grey, negative surfaces are in black. The arrows depict the normal to each triazole ring.

Let us consider that the vibrational properties of each molecular fragment (btr, NCS and Fe) in each spin state can be described by a mean single harmonic oscillator (rigid group model). This is a gross approximation which can, however, help rationalize the observed trends. The mean-square displacement amplitude corresponding to a harmonic oscillator is related to the vibration frequency by $\langle u^2 \rangle = \frac{h}{8\pi^2\mu v}\coth(h v/2k_B T)$, where μ is the reduced mass and v the oscillator frequency. $\langle u^2 \rangle$ is a decreasing function of the oscillator frequency, v. In this context, at constant temperature, the increase in the mean-square displacement amplitude in the HS state is related to a decrease in oscillator frequency and correlatively to a decrease in the stiffness of the crystal lattice; thus $v_{HS} < v_{LS}$. For this hypothetical harmonic oscillator, the vibrational entropy is a decreasing function of the oscillator frequency; thus $S_{HS} > S_{LS}$. We therefore predict, as a result of our structural analysis an increase in vibrational entropy upon LS-to-HS state change due to the external vibration modes. This positive contri-

bution to ΔS_{LH} from external modes could explain the remarkably high LS-to-HS total entropy change for [Fe(btr)$_2$-(NCS)$_2$]·H$_2$O.

All together, these results show the relevance of such a structural analysis by using high-resolution X-ray diffraction for getting new insights into the vibrational properties of spin-crossover materials.

Conclusions

This paper describes the structural properties of the LS and HS states of the spin-crossover complex [Fe(btr)$_2$-(NCS)$_2$]·H$_2$O and their modifications during the thermal (130 K) and the LIESST (15 K) spin transitions. The LIESST process at very low temperature and the metastable HS-2-to-LS relaxation have been described on the basis of spectroscopic and photomagnetic measurements. The very slow relaxation of the photostationary HS-2 state allows precise crystallographic studies of the metastable HS-2p and HS-2q states.

The X-ray diffraction measurements of the LS and HS states at rigorously the same temperature for the two conversions allow a precise description of the structural variations attributed to the spin transition, free from any disturbing thermal effect. Under these considerations, we showed that both HS-2 states obtained by thermal quenching from room temperature and by photoirradiation have the same molecular structures, within experimental limits of accuracy (less than 0.01 Å). In addition, our results suggest that the LIESST and the thermal spin transitions lead to the same structural variations of the iron coordination polyhedron: the Fe–N bond lengths extend by 0.18 and 0.20 Å on going from LS to HS, and the NCS group undergoes a reorientation of nearly 13°, which accounts for the extension of the crystallographic a axis. The HS→LS transition reduces the intermolecular Ow–Hw···N12 contacts in the crystallographic a direction.

We have shown in the present analysis that detailed vibrational properties related to the spin transition can be derived from X-ray diffraction measurements, providing high-resolution (in Q) data are measured. Systematically higher vibration amplitudes are observed in the HS state as compared to the LS state. For the btr group, the collective increase in vibration amplitude is perpendicular to each triazole ring and results from globally lower-frequency external vibration modes in the HS state. These might contribute significantly to ΔS_{HL}.

The thermal-expansion tensors for the HS and LS states exhibit a similar qualitative behaviour that parallels the specific layer crystal structure. In both spin states, the largest value of the thermal-expansion tensor is observed along the crystallographic a direction, that is, perpendicular to the structural layers. The corresponding thermal contraction is twice in the HS state with respect to the LS state. On the other side, the contraction is lower in the directions parallel to the layers. The spin transition in [Fe(btr)$_2$(NCS)$_2$]·H$_2$O is associated to large and anisotropic spontaneous strain, characterized by the tensor ε, whose eigenvalues correlate to an abrupt increase in the interlayer spacing and an overall contraction parallel to the layers.

Experimental Section

Sample Preparation: The btr ligand and its iron complex, [Fe(btr)$_2$-(NCS)$_2$]·H$_2$O, were synthesized as reported in the literature.[37] Single crystals, suitable for accurate crystallographic studies, were grown by slow solvent evaporation in aqueous solution. For consistency, single crystals of similar quality and size were used for all the experiments: single-crystal X-ray diffraction, optical and magnetic measurements.

Estimation of Crystal Heating during Photoexcitation: We report in this paper the physical properties of the light-induced metastable state of [Fe(btr)$_2$(NCS)$_2$]·H$_2$O obtained by using various laser excitation conditions (laser wavelength and power) for the photomagnetic, reflectivity and photocrystallographic measurements. It is of fundamental importance to address the question of crystal heating under such laser excitation. Whatever the experiment, it is commonly assumed and hoped that this sample heating is reduced, but no clear procedure has ever been proposed for estimating the temperature increase in the probed sample. We propose here a very simple empirical procedure for the case of photocrystallographic experiments.

Prior to any photocrystallographic measurement, it is of common practice to analyze comparatively the UV/Vis absorption spectra of the ground and light-induced excited states from which the excitation conditions (laser wavelength and power) are optimized. In the case of spin-crossover materials, excitation wavelength corresponding to the spin-allowed $^1A_1$ to $^1T_1$ or MLCT (Metal-to-Ligand Charge Transfer) absorption band is commonly chosen. Under such excitation conditions, the energy transferred to the sample partly induces the LS-to-HS excitation, but is also dissipated by emission of phonons. This latter process may raise the sample temperature by several tens of degrees, which could drastically damage it or cause false interpretations of the LIESST phenomenon. By using typical heat conduction properties (thermal conductivity) of molecular crystals, characteristics (stream diameter and velocity) and heat convection properties of the cooling N$_2$ or He gas stream (density, heat capacity, kinematic viscosity,...), and laser excitation parameters (penetration depth, linear absorption coefficient, laser power), the heat-transfer equations could be solved numerically, but not without difficulty, to attain the temperature increase profile in a single-crystal sample.[38] We propose here a simpler in situ empirical procedure for roughly estimating the maximum sample temperature increase induced by combined photoillumination and open-flow (N$_2$ or He) cooling systems, which is applicable to spin-crossover materials. We use the fact that on increasing temperature and passing through the LS-to-HS-1 spin transition (at $T = T_{1/2\uparrow}$), the cell parameters change significantly. We can therefore first record diffraction frames in the LS state as references. Then turn on the laser and measure the same diffraction frames as a function of laser power. Upon the LS-to-HS transition, a Bragg peak displacement is expected and usually observed. Therefore, a direct inspection of the diffraction pattern while increasing the laser power would indicate the point at which the laser heats the sample to a temperature which is above $T_{1/2\uparrow}$.

This procedure was applied to [Fe(btr)$_2$(NCS)$_2$]·H$_2$O. First we performed diffraction measurements on a single crystal of typical size (0.25 × 0.20 × 0.20 mm) in the LS state below $T_{1/2\uparrow}$ = 143 K. At

$T = 113$ K, the crystal was irradiated for 5 min at the optimum wavelength, $\lambda = 488$ nm, at a laser output power from 0 to 530 mW, and the diffraction pattern before and after excitation was compared. The laser power was calibrated beforehand by using a power-meter. For low laser power (below 530 mW), no changes appeared in the diffraction pattern, whereas at a laser power of 530 mW, a Bragg peak splitting was noticeable, which is indicative of partial LS-to-HS conversion (Figure 12). In other words, part of the crystal sample, most probably the fraction of the crystal just facing the laser, is at a temperature greater than $T_{1/2\uparrow}$, and the temperature increase is at least 32 K. If the laser excitation is stopped, the diffraction pattern returns quickly back to the corresponding LS state, consistent with the measurement temperature, $T = 113$ K, below $T_{1/2\downarrow}$. This proves that the crystal was not damaged by the laser, even at 530 mW.

It is well known that the specific heat is temperature-dependent, and the light-induced temperature may therefore be different at very low temperature ($T = 15$ K), at which the LS-to-HS-2p transition is induced in the present work. To check whether this was indeed the case, we performed another diffraction measurement with a starting temperature of 66 K in the LS state, just above T_{LIESST}. Again, the laser power was increased while measuring the diffraction pattern to check whether the LS-to-HS-1 transition could be reached. This would indicate a temperature increase of 77 K. Even with the highest laser power of 530 mW, no change was noticeable, which indicated that the temperature increase was indeed limited to below 77 K. Another similar procedure, although not carried out here, would be to prepare the system in the metastable HS-2 (HS-2p or HS-2q) state at very low temperature and inspect the diffraction pattern while increasing the laser power until the HS-2-to-LS LIESST relaxation is observed.

Under such circumstances, we are confident that during our light-induced LS-to-HS-2p experiment at $T = 15$ K, we did not heat our sample too much to surpass $T_{1/2\uparrow}$ and then quench our sample in the HS-2q state while turning off the laser. We propose that this procedure can be systematically checked prior to any photocrystallographic measurement. It is, however, purely empirical and does not allow a quantitative comparison with other experiments, since it is highly dependent on the current experimental excitation conditions used for the diffraction measurements.

Spectroscopic and Photomagnetic Measurements: Optical reflectivity properties were investigated with a custom-built reflectivity setup equipped with a CVI spectrometer, which allows the collection of both the reflectivity spectra within the 450–950 nm range at a given temperature and to follow the temperature dependence of the signal at a selected wavelength (± 2.5 nm) at 5–290 K. The analysis was performed on a thin layer of the powdered sample, without any dispersion in a matrix in the cooling mode from room temperature to 10 K and then warming up to 185 K. One has to keep in mind that reflectivity measurements yield surface information as compared to bulk information obtained from photomagnetic and diffraction results.

Magnetic susceptibility measurements were obtained by using an MPMS-55 Quantum Design SQUID magnetometer operating in the 2–340 K temperature range. The temperature was varied at a rate of 0.5 K min^{-1}. All magnetic data are plotted as $\chi_M T$ vs. T, the molar magnetic susceptibility χ_M being corrected for the diamagnetism of the closed-shell core and sample diamagnetism. The photomagnetic experiments were carried out by using a Spectra-Physics Kr+ laser (488 nm and 532 nm) or a diode laser (830 nm), with a power of 5 mW cm^{-2} at the sample surface, coupled through an optical fibre to the cavity of the SQUID magnetometer. The T_{LIESST} properties were measured in relation with the previously published method.[7] The sample was first slowly cooled to 10 K in the LS state and then irradiated with the laser. As soon as the photostationary limit was reached (no further increase in the mag-
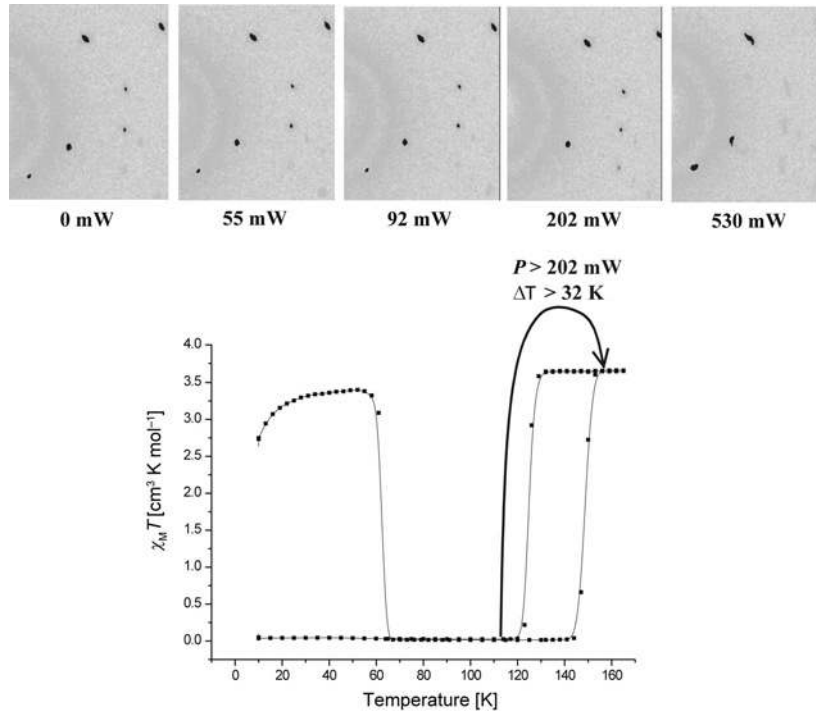

Figure 12. Top: the diffraction pattern as a function of laser excitation power at $\lambda = 488$ nm and $T = 113$ K. Note the change in the diffraction pattern at $P = 530$ mW. Bottom: schematic representation of the procedure for temperature increase estimation.

netic signal), the light irradiation was switched off and the magnetic signal recorded while the temperature was increased at a rate of 0.3 K min^{-1}. The T_{LIESST} value is given by the extreme of the curve $\partial\chi_M/\partial T$ vs. T. Thermomagnetic data were also collected on the quenched metastable HS state by using a rapid thermal cooling from room temperature directly to 10 K and deriving T_{TIESST} in the same way as T_{LIESST}.

X-ray Diffraction Measurements: Five data collections were performed in the different spin states: HS-1 and LS at 130 K within the thermal hysteresis loop, LS, HS-2p and HS-2q at 15 K (Figure 1) by using an Oxford Diffraction Xcalibur diffractometer with Mo-K_α radiation and equipped with a CCD Sapphire 2 detector. Diffraction experiments were performed by ω-scans by using a detector-to-sample distance of 50 mm at several detector 2θ positions. The cooling systems were an Oxford Diffraction He open flow Helijet and a N_2 open-flow cryostream. The temperature at the sample position was calibrated by using the tetragonal-to-orthorhombic structural phase transition of DyVO$_4$ at $T = 14$ K.[39] For the measurements with the N_2 open-flow cryostream, the temperature was calibrated with a thermocouple. Owing to the small size of the sample, the temperature gradient inside the crystal can be neglected, the flux being homogeneous and linear at the sample position. All diffraction peaks were integrated by using CRYSALIS software.[40] Cell parameters were derived with a least-squares refinement on all measured reflections. The crystal faces were indexed to perform analytical absorption corrections. The measured reflections were merged and reduced by using SORTAV.[41] There was no evidence

for structural phase transition or space group change after all spin-state changes (thermally induced and light-induced transitions). All structures were solved by direct methods and refined on F^2 using a similar strategy (SHELXL97).[42] Non-hydrogen atoms were refined anisotropically, hydrogen atoms were located on Fourier synthesis and refined isotropically without any constraint. More specific data collection and refinement details are given below and summarized in Table 6. We should stress the high resolution (θ_{max}) and low internal agreement factor (R_{int}) of all the experiments as direct pieces of evidence for the high quality and internal consistency of the measured data.

Low-Spin-State Data Collection at 15 K: The single-crystal sample was directly quenched to 70 K (above T_{LIESST}); the temperature was gradually decreased further to 15 K. According to the magnetic measurements, the thermal transition of [Fe(btr)$_2$(NCS)$_2$]·H$_2$O is complete; our measured sample corresponds to a purely LS state.

Metastable High-Spin States. Data Collection and Structural Refinement at 15 K: The diffraction measurement of the metastable HS-2 states is practically more difficult than that for the LS state, owing to the inherent HS-2-to-LS relaxation. Accordingly, controlled specific conditions had to be found in order to ensure at the same time a complete population of the metastable state and a quenched relaxation. As shown by the magnetic results, the relaxation is almost negligible at 15 K. The change in the unit cell volume in the course of the diffraction measurements could be an appropriate indicator to follow in situ and estimate the HS-2-to-

Table 6. Crystallographic and experimental data in the various spin states.

	LS at 15 K	HS-2q at 15 K	HS-2p at 15 K	LS at 130 K	HS-1 at 130 K
Formula	C$_{10}$H$_{10}$FeN$_{14}$OS$_2$	C$_{10}$H$_{10}$FeN$_{14}$OS$_2$	C$_{10}$H$_{10}$FeN$_{14}$OS$_2$	C$_{10}$H$_{10}$FeN$_{14}$OS$_2$	C$_{10}$H$_{10}$FeN$_{14}$OS$_2$
M_w	462.27	462.27	462.27	462.27	462.27
Space group	$C2/c$	$C2/c$	$C2/c$	$C2/c$	$C2/c$
a [Å]	11.1626(4)	10.9047(5)	10.874(2)	11.1971(8)	10.9580(5)
b [Å]	12.5839(6)	13.1125(6)	13.063(2)	12.5847(9)	13.1506(4)
c [Å]	12.7543(6)	13.162(1)	13.147(2)	12.7567(9)	13.1551(6)
β [°]	92.284(3)	90.883(8)	90.83(1)	92.307(6)	91.151(4)
V [Å^3]	1790.2(1)	1881.7(2)	1867.3(5)	1796.1(2)	1895.3(1)
Z	4	4	4	4	4
$\rho_{\text{calcd.}}$ [g cm^{-3}]	1.71	1.63	1.64	1.71	1.62
μ [mm^{-1}]	1.110	1.047	1.055	1.097	1.038
$T_{\text{min}}/T_{\text{max}}$	0.68/0.83	0.80/0.89	0.83/0.89	0.56/0.81	0.73/0.94
Crystal size [mm]	$0.32 \times 0.20 \times 0.13$	$0.36 \times 0.18 \times 0.12$	$0.23 \times 0.21 \times 0.14$	$0.60 \times 0.23 \times 0.12$	$0.41 \times 0.13 \times 0.06$
Data Collection					
λ [Å]	0.71073	0.71073	0.71073	0.71073	0.71073
T [K]	15	15	15	130	130
θ_{max} [°]	44.15	37.16	26.60	42.47	60.12
Total no. of reflections	26316	16975	1321	24072	66160
No. of indep. reflections	6407	3879	812	4124	12143
R_{int}[a]	0.034	0.033	0.045	0.025	0.032
Refinement					
Number of parameters	149	154	129	149	149
$R1$[b] (all data)	0.043	0.045	0.075	0.076	0.064
$R1$ [$I > 2\sigma(I)$]	0.033	0.027	0.065	0.049	0.035
$wR2$	0.084	0.057	0.172	0.135	0.091
GoF	1.04	0.80	1.29	1.07	0.92

[a] $R_{\text{int}} = \sum_H (N/N-1) \sum_i |I_i - \langle I \rangle| \Big/ \sum_H \sum_i I_i$.

[b] $R1 = \sum_H \big\| F_o | - | F_c \big\| \Big/ \sum_H | F_o |$, $wR2 = \left[\sum_H w\left(F_o^2 - F_c^2\right)^2 \Big/ \sum_H w\left(F_o^2\right)^2 \right]^{1/2}$, $\text{GoF} = \left[\sum_H w\left(F_o^2 - F_c^2\right)^2 \Big/ (n-p) \right]^{1/2}$.

LS relaxation rate in the course of the diffraction measurements, since the cell volume of the two spin states differ by more than 90 Å^3. We have already shown,[16] in the case of the HS-2q state, that the change in the cell volume as a function of time at 15 K exhibits a linear trend with an insignificant negative slope [$V(t) = 1880(3) – 0.002(5)t$]. The metastable state can therefore be considered stationary during the diffraction measurement.

According to our magnetic results, a complete HS-2q state can be trapped at 15 K by flash cooling from room temperature. The HS-2q crystal structure indicates a slight static disorder of the S atom which was refined at two independent positions. The two S positions have complementary refined occupancies of 0.0300(5) and 0.9700(5) for the minor and major positions, respectively. Such a disorder is not uncommon for the axial NCS ligands of spin-transition complexes.

The excitation conditions for the diffraction measurements of the HS-2p state were optimized according to the photomagnetic and spectroscopic results. The absorption band corresponding to the $^1A_1 \rightarrow {}^1T_1$ transition (LIESST effect) is centred at 550 nm. For the photocrystallographic measurements, the optimum conversion was found at $\lambda = 488$ nm ($P_{laser} = 46$ mW, exposure time = 30 s), aside the maximum of the absorption band, ensuring a rather good penetration depth in the single-crystal sample. Using these excitation conditions, a complete photoconversion was reached, since at the photostationary state, the Bragg peaks corresponding to the LS state were not noticeable any more. It is to be noted that the data quality of the HS-2p state is lower than that of the HS-2q state, as a result of an increase in crystal mosaicity after light irradiation and, correlatively, a smaller number of collected reflections. It was very difficult to obtain and measure this photoinduced state, and several crystals were destroyed during preliminary irradiation tests. The presently described data set is the best we could achieve. Contrary to the HS-2q crystal structure, we could not detect any S static disorder. Whether this is related to the lower data quality or attributed to a real structural difference between HS-2q and HS-2p is still an open question.

Low-Spin and High-Spin States. Data Collection and Structural Refinement at 130 K: We took advantage of the large thermal hysteresis centred at 134 K to measure the HS-1 and LS states at the same temperature, 130 K, in both spin states. This is an important issue since in this case thermal contraction effects do not interfere in the structural comparison. The measured samples were prepared in the appropriate spin state depending on their history. The HS-1 state was obtained directly by cooling from room temperature, whereas for the LS state, the sample was first cooled down to 100 K (below $T_{1/2\downarrow} = 123.5$ K) and then warmed up to 130 K. Contrary to the HS-2q state, no static disorder was noticed around S in either of the spin states.

CCDC-627392, -627393, -627394, -627395, -627396 contain the supplementary crystallographic data for this paper. These data can be obtained free of charge from The Cambridge Crystallographic Data Centre via www.ccdc.cam.ac.uk/data_request/cif.

Acknowledgments

[1] a) P. Gutlich, H. A. Goodwin (Eds.), *Topics in Current Chemistry, Vol. 233, 234, 235*, Springer-Verlag, Berlin, **2004**; b) P. Gütlich, A. Hauser, H. Spiering, *Angew. Chem. Int. Ed. Engl.* **1994**, *33*, 2024.

[2] P. Guionneau, M. Marchivie, G. Bravic, J.-F. Létard, D. Chasseau in *Topics in Current Chemistry, Vol. 234* (Eds: P. Gutlich, H. A. Goodwin), Springer-Verlag, Berlin, **2004**, p. 97.

[3] A. Bousseksou, K. Boukheddaden, M. Goiran, C. Conséjo, M.-L. Boillot, J.-P. Tuchagues, *Phys. Rev. B* **2002**, *65*, 172412.

[4] A. Hauser, *Chem. Phys. Lett.* **1986**, *124*, 543.

[5] S. Decurtins, P. Gütlich, C. P. Köhler, H. Spiering, *Chem. Phys. Lett.* **1984**, *105*, 1.

[6] J.-F. Létard, L. Capes, G. Chastanet, N. Moliner, S. Létard, J. A. Real, O. Kahn, *Chem. Phys. Lett.* **1999**, *313*, 115.

[7] J.-F. Létard, P. Guionneau, O. Nguyen, J. Sanchez Costa, S. Marcen, G. Chastanet, M. Marchivie, L. Goux-Capes, *Chem. Eur. J.* **2005**, *11*, 4582.

[8] A. Hauser, *Chem. Phys. Lett.* **1992**, *192*, 65.

[9] M. Marchivie, P. Guionneau, J.-F. Létard, D. Chasseau, *Acta Crystallogr., Sect. B* **2005**, *61*, 25.

[10] a) D. W. J. Cruickshank, *Acta Crystallogr.* **1956**, *9*, 757; b) D. W. J. Cruickshank, *Acta Crystallogr.* **1961**, *14*, 896.

[11] P. Guionneau, M. Marchivie, G. Bravic, J.-F. Létard, D. Chasseau, *J. Mater. Chem.* **2002**, *12*, 2546.

[12] a) M. Marchivie, P. Guionneau, J. A. K. Howard, G. Chastanet, J.-F. Létard, A. E. Goeta, D. Chasseau, *J. Am. Chem. Soc.* **2002**, *124*, 194–195; b) V. A. Money, I. Radosavljevic Evans, M. A. Halcrow, A. E. Goeta, J. A. K. Howard, *Chem. Commun.* **2003**, 158–159; c) E. J. MacLean, C. M. McGrath, C. J. O'Connor, C. Sangregorio, J. M. W. Seddon, E. Sinn, F. E. Sowrey, S. J. Teat, A. E. Terry, G. B. M. Vaughan, N. A. Young, *Chem. Eur. J.* **2003**, *9*, 5314–5322; d) N. Huby, L. Guérin, E. Collet, L. Toupet, J.-C. Ameline, H. Cailleau, T. Roisnel, T. Tayagaki, K. Tanaka, *Phys. Rev. B* **2004**, *69*, 020101; e) A. L. Thompson, A. E. Goeta, J. A. Real, A. Galet, M. C. Muñoz, *Chem. Commun.* **2004**, 1390–1391; f) V. Niel, A. L. Thompson, A. E. Goeta, C. Enachescu, A. Hauser, A. Galet, M. C. Muñoz, J. A. Real, *Chem. Eur. J.* **2005**, *11*, 2047–2060; g) J. Kusz, D. Schollmeyer, H. Spiering, P. Gütlich, *J. Appl. Crystallogr.* **2005**, *38*, 528–536; h) K. Ichiyanagi, H. Hebert, L. Toupet, H. Cailleau, P. Guionneau, J.-F. Létard, E. Collet, *Phys. Rev. B* **2006**, *73*, 060408.

[13] M. Marchivie, P. Guionneau, J.-F. Létard, D. Chasseau, J. A. K. Howard, *J. Phys. Chem. Solids* **2004**, *65*, 17.

[14] V. Legrand, C. Carbonera, S. Pillet, M. Souhassou, J.-F. Létard, P. Guionneau, C. Lecomte, *J. Phys. Conf. Ser.* **2005**, *21*, 73.

[15] S. Pillet, V. Legrand, H.-P. Weber, M. Souhassou, J.-F. Létard, P. Guionneau, C. Lecomte, *Z. Kristallogr.* **2007**, in press.

[16] V. Legrand, S. Pillet, M. Souhassou, N. Lugan, C. Lecomte, *J. Am. Chem. Soc.* **2006**, *128*, 13921.

[17] S. Pillet, C. Lecomte, C. F. Sheu, Y. C. Lin, I. J. Hsu, Y. Wang, *J. Phys. Conf. Ser.* **2005**, *21*, 221.

[18] J. S. Costa, P. Guionneau, J. F. Létard, *J. Phys. Conf. Ser.* **2005**, *21*, 67–72.

[19] W. Vreugdenhil, J. H. Van Diemen, R. A. G. De Graaff, J. G. Haasnoot, J. Reedijk, A. M. Van Der Kraan, O. Kahn, J. Zarembowitch, *Polyhedron* **1990**, *9*, 2971.

[20] S. Pillet, J. Hubsch, C. Lecomte, *Eur. J. Phys. B* **2004**, *38*, 541.

[21] a) J.-P. Martin, J. Zarembowitch, A. Bousseksou, A. Dworkin, J. G. Haasnoot, F. Varret, *Inorg. Chem.* **1994**, *33*, 6325; b) J.-P. Martin, J. Zarembowitch, A. Dworkin, J. G. Haasnoot, E. Codjovi, *Inorg. Chem.* **1994**, *33*, 2617.

[22] A. Desaix, O. Roubeau, J. Jeftic, J. G. Haasnoot, K. Boukheddaden, E. Codjovi, J. Linarès, M. Noguès, F. Varret, *Eur. Phys. J.* **1998**, *B6*, 183.

[23] S. Pillet, V. Legrand, M. Souhassou, C. Lecomte, *Phys. Rev. B* **2006**, *74*, 140101(R).

[24] J.-F. Létard, P. Guionneau, L. Rabardel, J. A. K. Howard, A. E. Goeta, D. Chasseau, O. Kahn, *Inorg. Chem.* **1998**, *37*, 4432.

[25] W. Morscheidt, J. Jeftic, E. Codjovi, J. Linares, A. Bousseksou, H. Constant-Marchado, F. Varret, *Meas. Sci. Technol.* **1998**, *9*, 1311.

[26] C. Enachescu, H. Constant-Machado, E. Codjovi, J. Linares, K. Boukheddaden, F. Varret, *J. Phys. Chem. Solids* **2001**, *62*, 1409.

[27] a) H. Spiering, E. Meissner, H. Köppen, E. W. Müller, P. Gütlich, *Chem. Phys.* **1982**, *68*, 65; b) P. Adler, L. Wiehl, E. Meissner, C. P. Köhler, H. Spiering, P. Gütlich, *J. Phys. Chem. Solids* **1987**, *48*, 517.

[28] J. Kusz, H. Spiering, P. Gütlich, *J. Appl. Crystallogr.* **2001**, *34*, 229.

[29] J. Kusz, H. Spiering, P. Gütlich, *J. Appl. Crystallogr.* **2000**, *33*, 201.

[30] N. W. Ashcroft, N. D. Mermin, *Solid State Physics*, New York: Holt, Rinehart and Winston, **1976**.

[31] R. Hundt, J. C. Schön, M. Jansen, *J. Appl. Crystallogr.* **2006**, *39*, 6.

[32] M. Sorai, S. Seki, *J. Phys. Chem. Solids* **1974**, *35*, 555–570.

[33] a) G. Brehm, M. Reiher, S. Schneider, *J. Phys. Chem., A* **2002**, *106*, 12024; b) K. L. Ronayne, H. Paulsen, A. Höfer, A. C. Dennis, J. A. Wolny, A. I. Chumakov, V. Schünemann, H. Winkler, H. Spiering, A. Bousseksou, P. Gütlich, A. X. Trautwein, J. McGarvey, *J. Phys. Chem. Chem. Phys.* **2006**, *8*, 4685.

[34] R. Zimmermann, E. König, *J. Phys. Chem. Solids* **1977**, *38*, 779–788.

[35] A. Bousseksou, H. Constant-Machado, F. Varret, *J. Phys. I Fr.* **1995**, *5*, 747–760.

[36] G. Molnar, V. Niel, A. B. Gaspar, J. A. Real, A. Zwick, A. Bousseksou, J. J. McGarvey, *J. Phys. Chem., B* **2002**, *106*, 9701–9707.

[37] W. Vreugdenhil, S. Gorter, J. G. Haasnoot, J. Reedijk, *Polyhedron* **1985**, *4*, 1769.

[38] a) T. M. Kuzay, M. Kazmierczak, B. J. Hsieh, *Acta Crystallogr., Sect. D* **2001**, *57*, 69; b) S. Kriminski, M. Kazmierczak, R. E. Thorne, *Acta Crystallogr., Sect. D* **2003**, *59*, 697.

[39] J. B. Forsyth, C. F. Sampson, *Phys. Lett. A* **1971**, *36*, 223–224.

[40] Oxford Diffraction, *CrysAlis CCD* and *CrysAlis RED*, Versions 1.171, Oxford Diffraction, Wroclaw, Poland, **2004**.

[41] R. H. Blessing, *J. Appl. Crystallogr.* **1989**, *22*, 396.

[42] G. M. Sheldrick, *SHELX97, Program for Structure Solution and Refinement*, University of Göttingen, Germany, **1997**.

[43] W. Hummel, J. Hauser, H. B. Bürgi, *J. Mol. Graphics* **1990**, *8*, 214.

[44] T. Balic Zunic, I. Vickovic, *J. Appl. Crystallogr.* **1996**, *29*, 305–306.